Polyethylene Crystal Orientation Induced by Block Copolymer Cylinders

Yueh-Lin Loo and Richard A. Register*

Department of Chemical Engineering, Princeton University, Princeton, New Jersey 08544-5263

Douglas H. Adamson

Princeton Materials Institute, Princeton University, Princeton, New Jersey 08540-5211

Received May 31, 2000

ABSTRACT: We examined the solid-state structures of two cylinder-forming semicrystalline diblock copolymers, where polyethylene forms the continuous matrix in both, using simultaneous small- and wide-angle X-ray scattering combined with transmission electron microscopy. The mesophase structure formed in the melt is largely retained upon cooling, whether the cylinders are glassy or rubbery during crystallization. Specimens in which the cylinders had been macroscopically oriented by flow revealed that the hexagonal packing of cylinders induces an unusual two-dimensional preferred orientation of the polyethylene crystals within the matrix. Specifically, the crystals tend to grow with their *b* axes parallel to the cylinder axes, while in the plane of the cylinder radii, the crystals tend to align their *c* axes parallel to the (10), (01), and (1$\bar{1}$) planes of the hexagonal macrolattice. By calculating various dimensions within the macrolattice, we conclude that the observed orientation allows the E crystals to best adopt their preferred thickness and spacing.

Introduction

Semicrystalline diblock copolymers can show solid-state structures quite distinct from those exhibited by crystallizable homopolymers, especially when microphase separation occurs prior to crystallization. Early studies of block copolymers that formed homogeneous[1,2] or weakly segregated[3] melts concluded that, regardless of composition, a lamellar morphology and ultimately a spherulitic superstructure are adopted upon crystallization. By contrast, even a weakly segregated mesophase can effectively confine the crystallizing block to nanometer-scale domains (such as spheres or cylinders) if the noncrystallizing majority block is vitreous at the temperature of crystallization.[4−7] However, the matrix need not be glassy to constrain crystallization of the other block, provided the interblock segregation is sufficiently strong. Recent experiments on strongly segregated diblocks reveal that crystallization can be guided by,[3,8] or entirely confined within,[9] the microdomains formed by interblock segregation in the melt, even when the domains formed by the noncrystallizing blocks remain fluid or rubbery at the onset of crystallization.

Block copolymer mesophases can also strongly influence the orientation of the crystals that form inside them. This effect was first noted by Douzinas and Cohen,[10] who studied segregated lamellar poly(ethylene-*block*-ethylethylene) diblocks, E/EE, where the EE block is above its glass transition during E block crystallization. Through X-ray pole figure analysis, they showed that the E chains crystallize with their stems generally *parallel* to the microdomain interfaces. Hamley et al.[7] used simultaneous small- and wide-angle X-ray scattering (SAXS/WAXS) to demonstrate a similar crystal stem orientation in a poly(vinylcyclohexane-*block*-ethylene) diblock, VCH/E, where the amorphous block is glassy ($T_g \cong 135$ °C) during E block crystallization. Systems where crystallization is confined within cylindrical microdomains have also been studied. Quiram et al.[5] demonstrated, through SAXS/WAXS, that the E chains within the cylindrical microdomains crystallize with their stems generally *perpendicular* to the cylinder axis. The seemingly disparate orientations in the cylindrical and lamellar morphologies can be understood by noting that both these orientations align the *b* axis—the fast growth direction for polyethylene—with the direction in which crystals can grow unobstructed by the microdomains formed by the amorphous block: along the cylinder axis in the cylindrical case and in the plane of the lamellae in the lamellar case. For the case where crystals are confined within cylinders (a VCH/E diblock), direct evidence for crystals growing along the cylinder axis has recently been obtained by transmission electron microscopy[11] (TEM).

Since block copolymer microdomains are easily aligned by the application of external fields, especially flow,[12] and do not readily lose their alignment when the field is removed, such microdomains represent a convenient way to control crystal orientation and yield mechanical and optical anisotropy in the solid state. While Quiram et al.[5] demonstrated that crystal orientation could be induced by confining the crystals *within* cylinders, we are interested here in whether the same approach is effective if the crystals are confined *outside* of the cylinders, i.e., whether nanoscale cylinders of amorphous material, formed through self-assembly in the melt, can induce orientation in the crystallizable matrix which surrounds them. Since crystals in the matrix of the cylindrical mesophase can also grow unobstructed only if they are aligned parallel to the cylinder axes, an orientation similar to that observed for crystallization within cylinders might be expected. As shown below, we indeed find this to be the case, but we also find that the hexagonal packing of cylinders induces a preferred crystal orientation in the plane of the cylinder radii, a phenomenon which does not occur when crystals are confined within cylinders.

* To whom correspondence should be addressed: Tel (609) 258-4691, e-mail register@princeton.edu.

10.1021/ma000962q CCC: $19.00
Published on Web 10/07/2000

Experimental Section

Synthesis and Molecular Characterization. *S/E 3/13:* The precursor to S/E 3/13, poly(styrene-*block*-high-1,4-butadiene), was synthesized using high-vacuum anionic polymerization in a 90/10 v/v cyclohexane/benzene mixture at room temperature. The molecular weight of the diblock was determined to be 15.9 kg/mol from the molecular weight of the first block (polystyrene, $M_n = 3240$ g/mol), as found by gel permeation chromatography (GPC), and the weight fraction of polystyrene in the styrene−butadiene diblock ($w_S = 0.204$), as determined via ^{1}H nuclear magnetic resonance (NMR). ^{1}H NMR also revealed a 7.5% 1,2 content in the butadiene block of the precursor. The polydispersity index was 1.03, and no terminated first block could be detected by GPC. The butadiene block was selectively saturated[13,14] (leaving the styrene block unaffected) using a nickel/aluminum catalyst in cyclohexane at 100 °C. Deuterium, instead of hydrogen, was used in the saturation reaction, but this is not material to the results discussed here. Fourier transform infrared spectroscopy (FT-IR) on the saturated polymer verified that there was no residual olefinic unsaturation in the sample. The resulting hydrogenous equivalent E block weight fraction, w_E, was calculated to be 0.802 (adding two hydrogens to each butadiene repeat unit on saturation). Because the crystallizable block is hydrogenated poly(high-1,4-butadiene), it is, strictly speaking, a random copolymer of ethylene and butene. By differential scanning calorimetry (DSC) at 10 °C/min (Perkin-Elmer DSC-7, calibrated with indium and mercury), S/E 3/13 shows a melting endotherm peak at 99 °C, and a room-temperature crystallinity, normalized by the weight fraction of polyethylene, of 32 wt % (taking the heat of fusion of fully crystalline polyethylene as 277 J/g[15]). This crystallinity is comparable to that of hydrogenated polybutadiene homopolymers of similar microstructure,[9] as both quantities are ultimately limited by the average run length of ethylene units between butene branch points. In addition, DSC cooling runs at 10 °C/min revealed that S/E 3/13 begins to crystallize at 82 °C. The crystallization exotherm is monomodal and narrow, spanning less than 10 °C, so primary crystallization is complete by 70 °C. Unfortunately, the polystyrene block glass transition could not be clearly discerned by DSC, due to the modest styrene content and to interference from lower-melting secondary E crystals. We estimate the glass transition temperature of the short S blocks in S/E 3/13 to be 50 °C, well below the freezing point of the E block, based on literature results for poly(styrene-*block*-dimethylsiloxane) diblocks of similar molecular weight and composition.[16] Poly(styrene-*block*-dimethylsiloxane) diblocks are appropriate for comparison because they have an even stronger segmental repulsion than poly(styrene-*block*-ethylene) block copolymers, so that in neither case are the polystyrene domains significantly plasticized by in-domain mixing with the other block.

VCH/E 6/15: The procedures followed for the synthesis and characterization of VCH/E 6/15 were largely similar to those for S/E 3/13; only differences are highlighted below. The precursor poly(styrene-*block*-high-1,4-butadiene) was synthesized in cyclohexane at 60 °C. Diblock $M_n = 21.3$ kg/mol; polydispersity index 1.06, with no terminated first block; weight fraction of polystyrene $w_S = 0.279$; vinyl content in the butadiene block 8.3%. To obtain complete saturation of both blocks (with H_2), a heterogeneous Pd^0 on $CaCO_3$ catalyst was employed.[14,17] The resulting VCH/E 6/15 diblock was calculated to have $w_E = 0.717$; peak $T_m = 104$ °C; room-temperature E block crystallinity 32 wt %; crystallization onset at 82 °C (10 °C/min).

Morphological Characterization. To assess the morphologies of S/E 3/13 and VCH/E 6/15, one-dimensional SAXS data were collected using an Anton-Paar compact Kratky camera connected to a position-sensitive detector (Braun OED-50M). The raw data were reduced using previously reported procedures[18] to obtain profiles of desmeared absolute intensity as a function of scattering vector $q = (4\pi/\lambda) \sin \theta$, where λ represents the incident radiation wavelength and 2θ is the scattering angle. A hot stage[19] was used to acquire SAXS profiles at elevated temperatures.

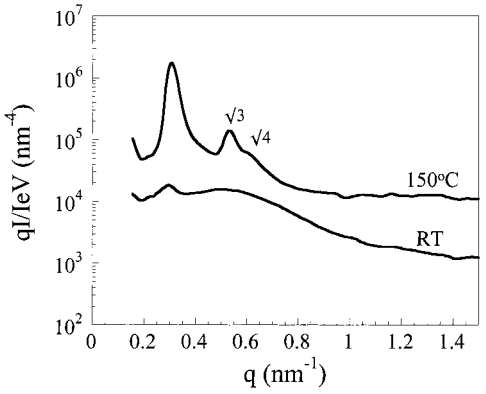

Figure 1. One-dimensional SAXS profiles of S/E 3/13 taken in the melt at 150 °C (top, intensity ×10 for clarity) and fully crystallized at room temperature (bottom).

Flow alignment of S/E 3/13 and VCH/E 6/15 was obtained with a lubricated channel die.[20,21] Molding was conducted at temperatures where both blocks are fluid (130 °C for S/E 3/13 and 160 °C for VCH/E 6/15). The mold was held isothermally for 30 min before it was removed from the hot press and allowed to cool in air to room temperature at approximately 20 °C/min. The molded strips were then cut accordingly for two-dimensional SAXS/WAXS experiments, performed with an evacuated Statton pinhole camera.[22] SAXS and WAXS images were collected simultaneously, from the same location on each specimen, using Kodak image plates read with a Molecular Dynamics Phosphorimager SI scanner. Azimuthal traces were then generated from the SAXS and WAXS patterns to examine the crystal orientation with respect to the flow-aligned cylinders. Cu Kα radiation was used for all X-ray measurements.

Real-space images of oriented S/E 3/13 (same strip examined by 2D SAXS/WAXS) were obtained by transmission electron microscopy (TEM). Slivers of the oriented strip were block-stained in 0.5 wt % RuO_4 aqueous solution (Electron Microscopy Sciences, used as received) for 12−24 h. Details of the staining and ultramicrotoming procedures can be found elsewhere.[11] Since styrene reacts preferentially with RuO_4[23], the cylindrical microdomains appear black in the micrographs. Similar attempts to examine VCH/E 6/15 by TEM did not produce satisfactory images of the cylinders; the VCH cylinders and E crystals are very difficult to distinguish from each other, as both take up RuO_4 far more slowly than the amorphous E regions.

Results and Discussion

Solid-State Morphology of S/E 3/13 Following Crystallization. In the melt, S/E 3/13 exhibits a sharp primary peak at $q^* = 0.314$ nm^{-1} and higher-order structure factor peaks at q/q^* ratios of $\sqrt{3}$ and $\sqrt{4}$ in its SAXS profile, indicating that the S cylinders are packed in a hexagonal array[24] within the E matrix (see top profile in Figure 1). We determined the order−disorder transition temperature to be 158 ± 1 °C from SAXS heating runs, suggesting that S/E 3/13 is moderately segregated at the E freezing point. Upon cooling below the freezing point of S/E 3/13, the higher-order structure factor peaks (see lower curve of Figure 1, obtained at room temperature after cooling from the melt at approximately 10 °C/min) are overwhelmed by a broad hump. The shape and position of this hump are similar to those exhibited by fully crystallized poly(high-1,4-butadiene) homopolymer;[1] hence, we attribute the broad hump to the scattering from E crystallites. The primary peak at room temperature ($q^* = 0.291$ nm^{-1}) is at slightly lower q than at 150 °C, due to movement of the peak in the melt prior to crystallization. (Increas-

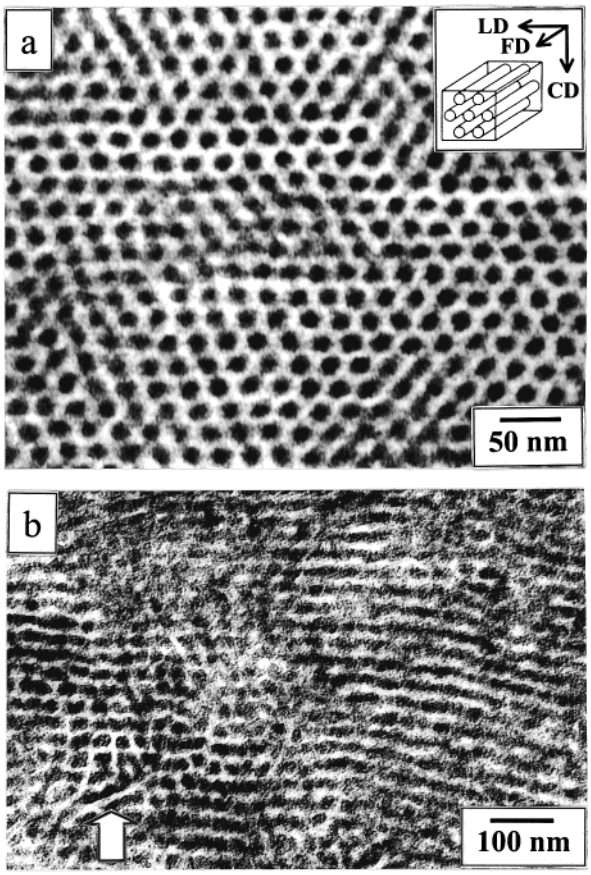

Figure 2. TEM micrographs of aligned S/E 3/13, S cylinders stained dark. A schematic of the alignment of the cylindrical microdomains imposed by extensional flow is shown in the inset. (a) Electron beam along the flow direction (FD); (b) electron beam along the constraint direction (CD). Arrow highlights nearly vertical white stripes which appear to be E crystals cutting through S cylinders.

ing χ with decreasing temperature causes the equilibrium microdomain spacing to increase as temperature is reduced.) The primary peak intensity is also reduced upon E block crystallization, due to the reduction in electron density contrast accompanying the density change. However, the presence of a macrolattice peak at room temperature strongly suggests that the melt morphology is retained on crystallization.[9]

Figure 2 contains TEM micrographs taken on S/E 3/13 after it had been aligned and crystallized in the channel die. (See Experimental Section for details of processing history.) Figure 2a represents a cross section perpendicular to the flow direction (FD; see inset for schematic of alignment due to extensional flow) while Figure 2b is a lower magnification image of a cross section perpendicular to the constraint direction (CD). The TEM micrographs confirm what the static SAXS data in Figure 1 imply: that crystallization of the E blocks largely occurs in place, without eradicating the previously established melt morphology. Although the cylindrical morphology is generally retained on crystallization, some distortion of the microdomains is evident in the micrographs. In particular, the left portion of Figure 2b shows several nearly-vertical white stripes which appear to be E crystals cutting through the S cylinders at nearly right angles (highlighted with a white arrow). Since the glass transition temperature of the S microdomains is approximately 30 °C below the freezing point of the E block, such deformation of the cylinders can occur during crystallization. However, two-dimensional SAXS shows that these local distortions do not destroy the long-range order within the sample. In Figure 3a, the two spots on the meridian when the X-ray beam is perpendicular to the (horizontal) cylinder axis indicate that even after crystallization, the polystyrene cylinders still have their axes aligned in the direction of flow. Furthermore, the six spots observed in the SAXS pattern when the X-ray beam is parallel to the cylinder axis (Figure 3c) indicate that the hexagonal lattice packing is also preserved on cooling. The observation of a six-spot pattern with the beam along the flow direction agrees with prior findings[5,21,25] that the planar extensional flow imposed by the channel die not only aligns the cylinder axes in the flow direction but also can generate a quasi-single-crystal orientation in the specimen, where the (10) planes of the hexagonal macrolattice have their normals aligned with the loading direction.

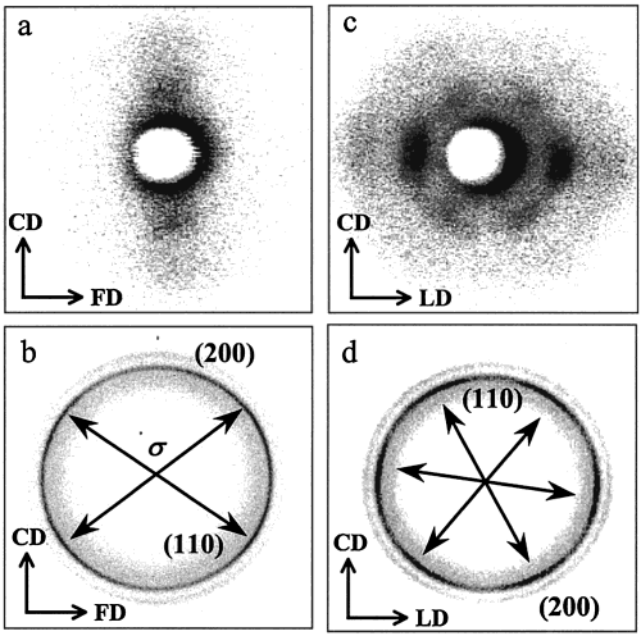

Figure 3. Two-dimensional SAXS (top, panels a and c) and WAXS (bottom, panels b and d) patterns of S/E 3/13 taken at room temperature following crystallization: (a, b) X-ray beam along the loading direction (LD); (c, d) X-ray beam along the flow direction (FD). Planes (*hk*0) indicated on the WAXS patterns correspond to the orthorhombic E unit cell.

Polyethylene Crystal Orientation in Flow-Aligned S/E 3/13. Figure 3b,d contains two-dimensional WAXS patterns acquired simultaneously with the corresponding SAXS patterns. The WAXS pattern taken with the X-ray beam in the loading direction (Figure 3b) reveals preferential orientation of the orthorhombic E crystals: for the (110) reflection, we observe four off-axis regions of high-intensity split by an azimuthal angle $\sigma = 115 \pm 1°$ across the meridian, while the (200) reflection exhibits two intense arcs on the meridian. The SAXS and WAXS patterns in Figure 3a,b match up precisely with the results of Quiram et al.[5] for diblocks where the E block crystallizes *within* cylinders; the E crystal stems are preferentially oriented perpendicular to the cylinder axes, giving a theoretical $\sigma = 116°$, while the *b* axes of the E crystals lie preferentially parallel to the cylinder axes. Thus, whether the E crystals are inside or outside the cylinders, the fact that crystals can grow uninterrupted only if they grow parallel to the

cylinder axes leads to the same type of orientation. Indeed, there is precedent for this type of orientation even when the cylinders are much larger than the thickness of the crystals:[22] for isotactic polypropylene (*i*PP) reinforced with unidirectional fibers of order 10 μm diameter, made from either glass or polyacrylonitrile-based carbon (neither of which nucleates *i*PP), the crystal stems preferentially orient perpendicular to the fiber axes because the interfiber spacing is significantly smaller than the average spherulite diameter in the unreinforced *i*PP. Moreover, as is true when the crystals are confined within block copolymer cylinders,[5] the amorphous block need not be glassy to obtain this preferential orientation: the interblock segregation present in S/E 3/13 is sufficient to largely preserve the cylinders throughout crystallization despite their fluidity.

By contrast, the WAXS pattern in Figure 3d shows a surprising result: the polyethylene crystals are preferentially oriented in two dimensions; i.e., not only do the crystals have their *b* axes aligned with the cylinder axes, they also show preferential orientation in the plane of the cylinder radii. With the X-ray beam along the flow direction, both the (110) and (200) reflections show a 6-fold intensity modulation (highlighted with arrows in Figure 3d). Such a modulation is not observed when the crystallites are confined *within* cylinders, as there is nothing to significantly perturb the uniaxial symmetry of a single cylinder.[26] In the matrix of the hexagonal mesophase, however, the regions that the crystals can occupy are demarcated by adjacent cylinders, which are packed in a hexagonal arrangement and hence produce this modulation.

Azimuthal traces were generated from the SAXS (first-order, (10), reflection of the hexagonal macrolattice) and WAXS (E unit cell (110) reflection) patterns of Figure 3c,d. To produce an estimate of the degree of crystal orientation from the WAXS data, the contribution of the amorphous E and S was first determined at each azimuthal position from the intensities at slightly higher and lower angle than the E (110) reflection and then subtracted from the data. Background subtraction was not applied to the SAXS data.[27] The resulting azimuthal traces, shown in Figure 4, clearly show that the 6-fold maxima in the SAXS and WAXS patterns are in azimuthal register. Similar SAXS and WAXS patterns were acquired from several different locations on the molded strip, and all showed azimuthal registration of the maxima, indicating the generality of this orientation for S/E 3/13. The azimuthal registry of the macrolattice (10) spots and the E crystallite (110) and (200) spots indicates that the *c* axes of the polyethylene crystal tend to align with the (10) planes (and equivalent (01) and ($1\bar{1}$) planes) of the two-dimensional hexagonal macrolattice formed by the cylindrical microdomains. However, the moderate peak-to-valley intensity ratio ($\approx$1.6) in the azimuthal WAXS trace indicates that other orientations of the crystal stems are certainly present.

While the SAXS and WAXS data clearly show the manner in which both the S microdomains and E crystals are oriented, since both are ensemble-average measurements, they do not reveal how the S cylinders produce this orientation in *adjacent* crystals. We can, however, make an inference about the mechanism by comparing the relevant dimensions in the solid-state structure. Various dimensions of the hexagonal macrolattice at room temperature, drawn to scale in Figure 5, were calculated from the SAXS primary peak position

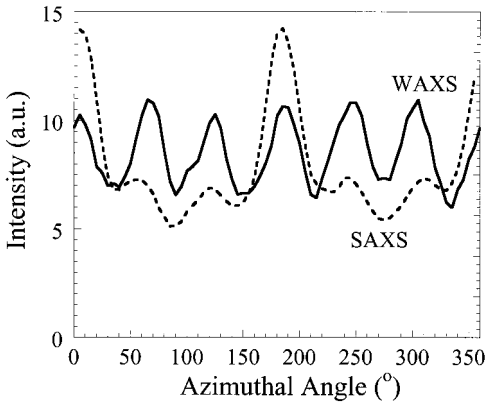

Figure 4. Azimuthal traces of the primary reflection of the hexagonal macrolattice (dashed curve) and the polyethylene (110) reflection (solid curve) for flow-aligned S/E 3/13, generated from the SAXS and WAXS patterns in Figure 3. Zero azimuthal angle is taken as a horizontal ray pointing right in Figure 3c,d, with azimuthal angle increasing clockwise. The intensities are integrated over the *q* range spanning the relevant reflections, and while the intensities are presented in arbitrary units, the zero of intensity has significance: zero total intensity for the SAXS data and zero net intensity (above the background contributed by the amorphous E and S) for the WAXS data.

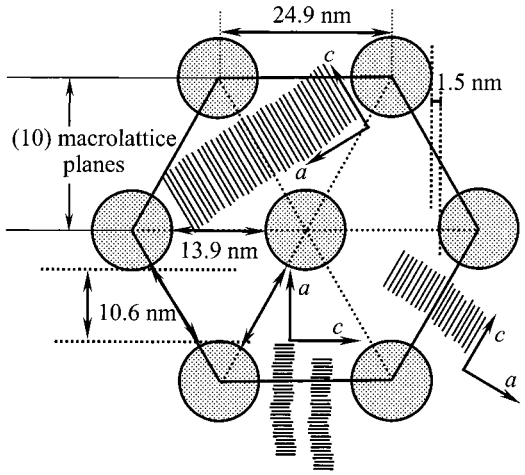

Figure 5. Proposed schematic cross section of oriented S/E 3/13 perpendicular to the flow direction, drawn to scale. Shaded circles indicate the cross sections of S cylinders, with the center-to-center spacing between adjacent cylinders equal to 24.9 nm. The short parallel lines indicate E crystal stems, which preferentially align with the lines of centers connecting adjacent cylinders. These lines of centers define the (10), (01) and (11) planes of the hexagonal macrolattice. The *a* and *c* axes are indicated for crystals in the three orientations which produce the six-spot SAXS pattern of Figure 3d (*b* axis out of the page, though all the axes show some distribution of orientation[27]).

and from the known weight fractions and densities of S and E.[28] The edge-to-edge distance between two cylinders in the (10) planes, which is the direction of the crystal stems, is 13.9 nm. Coincidentally, the average crystal thickness of hydrogenated poly(high-1,4-butadiene) homopolymer is approximately 5 nm, with a 13 nm average repeat distance.[1] As this thickness is dictated by the sequences of crystallizable ethylene units between ethyl branch defects, it is largely independent of thermal history.[29] The E crystal stems are drawn in Figure 5 in a manner consistent with the preferred orientation observed experimentally (*a* and *c* axes indicated, *b* axis generally perpendicular to the page,

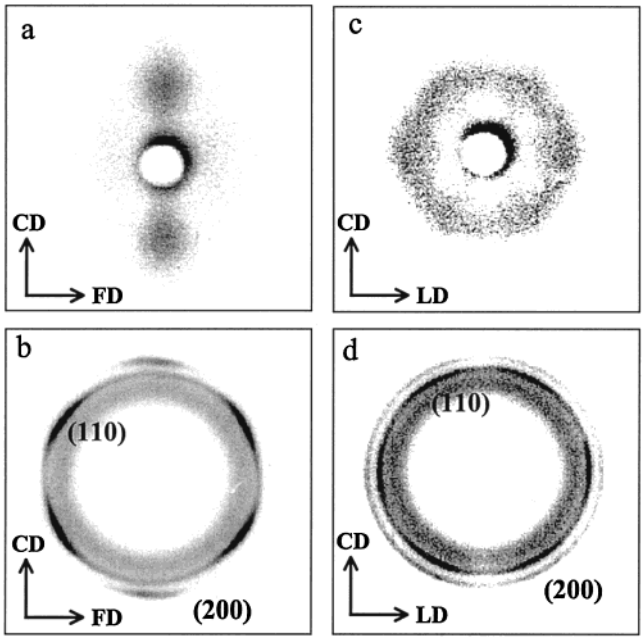

Figure 6. Two-dimensional SAXS (top, panels a and c) and WAXS (bottom, panels b and d) patterns of VCH/E 6/15 taken at room temperature following crystallization: (a, b) X-ray beam along the loading direction (LD); (c, d) X-ray beam along the flow direction (FD). Planes (*hk*0) indicated on the WAXS patterns correspond to the orthorhombic E unit cell.

allowing the crystals to grow long in the *b* axis direction). Inserting the E crystals into the hexagonal mesophase in this fashion allows one "average" E crystal and its associated amorphous material (or perhaps two thin crystals, given the broad distribution of crystal thicknesses in such random copolymers[30]) to fit comfortably between the S cylinders, though it restricts the transverse dimension of the crystals (along the *a* axis). Orientations that would allow the crystals to extend far along the *a* axis would constrain the dimensions of the crystals in the thickness direction; for example, aligning the *c* axis of the E crystals perpendicular to the (10) macrolattice planes provides a space for the crystals of only 10.6 nm in the *c* axis direction, a distance demarcated by planes tangent to the cylinder surfaces. Indeed, a similar orientation of the crystals was recently proposed by Liu et al.[31] in blends of polytetrahydrofuran with a poly(tetrahydrofuran-*block*-methyl methacrylate) diblock, PTHF/PMMA, containing glassy PMMA cylinders at the PTHF freezing point. However, since only isotropic samples were examined, the unusual modulation of the WAXS pattern seen for S/E 3/13 in Figure 3d was not observed.

Polyethylene Crystal Orientation in Flow-Aligned VCH/E 6/15. To examine the generality of this mode of orientation, we studied a second polyethylene-containing diblock copolymer, VCH/E 6/15. Here, the cylinder-forming block is poly(vinylcyclohexane), whose glass transition temperature is well above the freezing point of the E block, so in contrast to S/E 3/13, the cylinders in VCH/E 6/15 are glassy throughout crystallization. The 2D SAXS and WAXS patterns for flow-aligned VCH/E 6/15, shown in Figure 6, are largely similar to those shown for S/E 3/13 in Figure 3. In fact, the arcs in the WAXS patterns for VCH/E 6/15 are more crisply defined than for S/E 3/13, indicating a higher degree of crystal orientation. This is confirmed by the azimuthal traces shown in Figure 7; again, the SAXS and WAXS peaks are in azimuthal registry, but for VCH/E 6/15, the WAXS peak-to-valley ratio is approximately 2.8 (vs 1.6 for S/E 3/13).

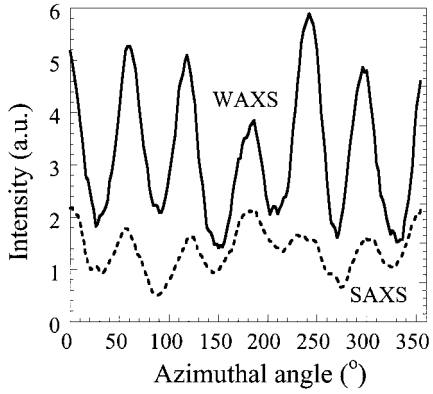

Figure 7. Azimuthal traces of the primary reflection of the hexagonal macrolattice (dashed curve) and the polyethylene (110) reflection (solid curve) for flow-aligned VCH/E 6/15, generated from the SAXS and WAXS patterns in Figure 6 following the procedure employed for Figure 4.

One-dimensional SAXS patterns for VCH/E 6/15 in the melt and solid states (not shown) were quite similar to those for S/E 3/13 in Figure 1, with a room-temperature $q^* = 0.306$ nm^{-1} for VCH/E 6/15. The relevant macrolattice dimensions are thus similar to those shown in Figure 5 for S/E 3/13; the edge-to-edge separation of adjacent cylinders is 10.7 nm (vs 13.9 nm for S/E 3/13), and the unobstructed regions between (10) macrolattice planes are 7.5 nm thick (vs 10.6 nm for S/E 3/13). We can thus suggest two possibilities for why VCH/E 6/15 shows a higher degree of crystal orientation than S/E 3/13. The first is simply that the glassy VCH cylinders are more difficult for the growing E crystals to disrupt than are the rubbery S cylinders, so local structural distortions of the type seen in Figure 2b are reduced. The second is that the smaller dimensions in VCH/E 6/15 produce a more stringent discrimination between the different possible crystal orientations. Indeed, we would anticipate that as the intercylinder spacing is increased (by making the block copolymer molecular weight much larger), this crystal orientation in the plane of the cylinder radii should disappear.

Conclusions

Hexagonally packed cylindrical microdomains can produce preferential orientation, in two dimensions, of crystals that form between the cylinders. Macroscopically aligning the cylinders yields a macroscopic orientation of the *b* axes of the E crystals parallel to the cylinder axes. Furthermore, the E crystals have their *c* axes preferentially aligned along the (10) planes of the hexagonal macrolattice in the plane of the cylinder radii. Orientation of the E crystals in this second dimension is not observed when crystallization is confined *within* cylinders and represents an additional mode of control which block copolymer mesophases can exert upon crystals that form within them. We attribute the observed orientation in this second dimension to the fact that the edge-to-edge distance between cylinders and the E crystal long spacing are comparable, such that this alignment allows the E crystal stems to best adopt their unconstrained lengths.

Acknowledgment. Financial support for this study came from the National Science Foundation, Polymers

Program (DMR-9711436). D.H.A. was supported by the National Science Foundation through the Princeton Center for Complex Materials (NSF-DMR-9400362, -9809483).

References and Notes

(1) Rangarajan, P.; Register, R. A.; Fetters, L. J. *Macromolecules* **1993**, *26*, 4640.
(2) Rangarajan, P.; Register, R. A.; Adamson, D. H.; Fetters, L. J.; Bras, W.; Naylor, S.; Ryan, A. J. *Macromolecules* **1995**, *28*, 4932.
(3) Quiram, D. J.; Register, R. A.; Marchand, G. R.; Ryan, A. J. *Macromolecules* **1997**, *30*, 4551.
(4) Cohen, R. E.; Cheng, P. L.; Douzinas, K.; Kofinas, P.; Berney, C. V. *Macromolecules* **1990**, *23*, 324.
(5) Quiram, D. J.; Register, R. A.; Marchand, G. R.; Adamson, D. H. *Macromolecules* **1998**, *31*, 4891.
(6) Weimann, P. A.; Hajduk, D. A.; Chu, C.; Chaffin, K. A.; Brodil, J. C.; Bates, F. S. *J. Polym. Sci., Part B: Polym. Phys.* **1999**, *37*, 2053.
(7) Hamley, I. W.; Fairclough, J. P. A.; Terrill, N. J.; Ryan, A. J.; Lipic, P. M.; Bates, F. S.; Towns-Andrews, E. *Macromolecules* **1996**, *29*, 8835.
(8) Quiram, D. J.; Register, R. A.; Marchand, G. R.; Ryan, A. J. *Macromolecules* **1997**, *30*, 8338.
(9) Loo, Y.-L.; Register, R. A.; Ryan, A. J. *Phys. Rev. Lett.* **2000**, *84*, 4120.
(10) Douzinas, K. C.; Cohen, R. E. *Macromolecules* **1992**, *25*, 5030.
(11) Loo, Y.-L.; Register, R. A.; Adamson, D. H. *J. Polym. Sci., Part B: Polym. Phys.* **2000**, *38*, 2564.
(12) Keller, A.; Pedemonte, E.; Willmouth, F. M. *Nature* **1970**, *225*, 538.
(13) Hahn, S. F. *J. Polym. Sci., Part A: Polym. Chem.* **1992**, *30*, 397.
(14) Adams, J. L.; Quiram, D. J.; Graessley, W. W.; Register, R. A. *Macromolecules* **1997**, *31*, 201.
(15) Brandrup, J., Immergut, E. H., Eds.; *Polymer Handbook*, 3rd ed.; Wiley: New York, 1989; p V-16.
(16) Lu, Z.-H.; Krause, S. *Macromolecules* **1982**, *15*, 112.
(17) Gehlsen, M. D.; Bates, F. S. *Macromolecules* **1994**, *27*, 3611.
(18) Register, R. A.; Bell, T. R. *J. Polym. Sci., Part B: Polym. Phys.* **1992**, *30*, 569.
(19) Adams, J. L.; Quiram, D. J.; Graessley, W. W.; Register, R. A.; Marchand, G. R. *Macromolecules* **1996**, *29*, 2929.
(20) Khan, S. A.; Larson, R. G. *Rheol. Acta* **1991**, *30*, 1.
(21) Lee, H. H.; Register, R. A.; Hajduk, D. A.; Gruner, S. M. *Polym. Eng. Sci.* **1996**, *25*, 6137.
(22) Dean, D. M.; Rebenfeld, L.; Register, R. A.; Hsiao, B. S. *J. Mater. Sci.* **1998**, *33*, 4797.
(23) Sawyer, L. C.; Grubb, D. T. *Polymer Microscopy*, 2nd ed.; Chapman and Hall: New York, 1996.
(24) Hashimoto, T.; Fujimura, M.; Kawai, H. *Macromolecules* **1980**, *13*, 1660.
(25) Scott, D. B.; Waddon, A. J.; Lin, Y.-G.; Karasz, F. E.; Winter, H. H. *Macromolecules* **1992**, *25*, 4175.
(26) Matsen, M. W.; Bates, F. S. *J. Chem. Phys.* **1997**, *106*, 2436.
(27) The unequal intensities of the six spots in the SAXS pattern of Figure 3c and the corresponding azimuthal trace (Figure 4) indicate a slight misalignment of the cylinder axes with respect to the incident X-ray beam. This could result either from imperfect orientation in the channel die or from a slight misalignment in specimen mounting and is frequently encountered in block copolymers oriented and examined similarly.[5] Since the E crystals have a broader orientational distribution than the S cylinders, small misalignments are inconsequential for the WAXS data, and the six peaks in the WAXS azimuthal trace (Figure 4) are of very similar intensity.
(28) The volume fraction of polystyrene at room temperature was calculated to be 0.176 based on an S domain density[32] of 1.048 g/cm^3 and an E domain density[29] of 0.910 g/cm^3.
(29) Howard, P. R.; Crist, B. *J. Polym. Sci., Part B: Polym. Phys.* **1989**, *27*, 2269.
(30) Crist, B.; Howard, P. R. *Macromolecules* **1999**, *32*, 3057.
(31) Liu, L.-Z.; Chu, B. *J. Polym. Sci., Part B: Polym. Phys.* **1999**, *37*, 779.
(32) Richardson, M. J.; Savill, N. G. *Polymer* **1977**, *18*, 3.

MA000962Q